Energy & Environmental Science

COMMUNICATION

Cite this: *Energy Environ. Sci.*, 2016, **9**, 478

Received 11th November 2015,
Accepted 23rd December 2015

DOI: 10.1039/c5ee03440j

www.rsc.org/ees

Vertically oriented cobalt selenide/NiFe layered-double-hydroxide nanosheets supported on exfoliated graphene foil: an efficient 3D electrode for overall water splitting†

Yang Hou, Martin R. Lohe, Jian Zhang, Shaohua Liu, Xiaodong Zhuang and Xinliang Feng*

Developing cost-effective electrocatalysts for both oxygen evolution reaction (OER) and hydrogen evolution reaction (HER) in basic media is critical to renewable energy conversion technologies. Here, we report a ternary hybrid that is constructed by *in situ* growth of cobalt selenide ($Co_{0.85}Se$) nanosheets vertically oriented on electrochemically exfoliated graphene foil, with subsequent deposition of NiFe layered-double-hydroxide by a hydrothermal treatment. The resulting 3D hierarchical hybrid, possessing a high surface area of 156 $m^2 g^{-1}$ and strong coupling effect, exhibits excellent catalytic activity for OER, which only requires overpotentials of 1.50 and 1.51 V to attain current densities of 150 and 250 mA cm^{-2}, respectively. These overpotentials are much lower than those reported for other non-noble-metal materials and Ir/C catalysts. The hybrid also efficiently catalyzes HER in base with a current density of 10 mA cm^{-2} at an overpotential of −0.26 V. Most importantly, we achieve a current density of 20 mA cm^{-2} at 1.71 V by using the 3D hybrid as both a cathode and an anode for overall water splitting, which is well comparable to the integrated performance of Pt/C and Ir/C catalysts.

Broader context

Electrochemical overall water splitting has received considerable attention as a promising strategy to convert the electrical output from renewable resources into chemical fuels, namely oxygen and hydrogen. A key challenge related to overall water splitting is the quest to develop highly-active and low-cost electrocatalysts with superior durability for both the oxygen evolution reaction and the hydrogen evolution reaction to replace noble metal catalysts. However, to date, only a few materials have been able to catalyse both reactions in the same electrolyte. This study reports on a three-dimensional (3D) strongly coupled ternary hybrid electrode, in which nonstoichiometric cobalt selenide ($Co_{0.85}Se$) nanosheet array and NiFe layered-double-hydroxide (NiFe-LDH) are successively grown on the electrochemically exfoliated graphene (EG) foil. As the result of the 3D nanoarchitecture with high surface area (156 $m^2 g^{-1}$), a strong coupling effect among different components, and open-channels for facile electrolyte transport, the resulting ternary hybrid shows excellent electrocatalytic activity for overall water splitting and stability in basic media. The work represents a significant step towards the development of novel type of 3D ternary hybrid electrocatalysts for electrochemical overall water splitting.

Electrochemical water splitting is one of the most attractive methods for efficient renewable energy production by converting electrical energy into chemical energy stored by hydrogen fuels.[1,2] The water electrolysis reaction consists of two half reactions: oxygen evolution reaction (OER) and hydrogen evolution reaction (HER).[3–5] An effective electrocatalyst is needed to reduce the energy barrier and thus to enhance the energy conversion efficiency. Although noble-metal materials (such as Ir-based for OER and Pt-based for HER) are currently the state-of-the-art catalysts to split water, their high cost and low earth abundance limit their wide-spread use. In the past few years, significant progress has been made in developing non-precious metal catalysts with high activity, such as perovskite oxides,[6,7] transition metal oxides/hydroxides[8] for the OER in basic electrolytes, and transition metal sulfides/phosphides/nitrides/carbides/selenides/borides[9–16] for the HER in acidic electrolytes. Considering sustained overall water splitting for practical applications, the electrocatalysts for OER and HER must be operated in the same electrolyte, especially in alkaline solution.[17] However, it remains challenging for most of the earth-abundant catalysts (*e.g.* MoS_2) because a highly active catalyst in an acidic electrolyte may not be active in a basic electrolyte.[18] Despite little progress,[2,15,19–21] novel electrocatalysts with high catalytic activity and stability that are capable of catalyzing both HER and OER in alkaline solution are in great demand.

As a typical transition metal dichalcogenide, cobalt selenide has recently received extensive attention owing to its excellent catalytic performance, high chemical stability, and low cost.[22] Compared with well-reported $CoSe_2$ nanobelts for various applications (such as solar cells[23] and water splitting (OER in basic media and HER in acid media)[24,25]), the nonstoichiometric

Department of Chemistry and Food Chemistry & Center for Advancing Electronics Dresden (CFAED), Technische Universitaet Dresden, 01062 Dresden, Germany. E-mail: xinliang.feng@tu-dresden.de

† Electronic supplementary information (ESI) available. See DOI: 10.1039/c5ee03440j

phase of two-dimensional cobalt selenide ($Co_{0.85}Se$) has been rarely studied.[26] The nonstoichiometric $Co_{0.85}Se$ has intrinsic half-metallic character (high conductivity) owing to the presence of an overlap between Co 3d and Se 4p spin-up (alpha) electrons, making it uniquely advantaged as an electrocatalyst material.[27] In particular, the nonstoichiometric $Co_{0.85}Se$ nanosheets with abundant exposed surface active sites can be beneficial for the overall water splitting in alkaline solution, where the OH^- can attach to $Co_{0.85}Se$ nanosheets due to the strong electrostatic affinity to the local positively charged Co^{2+} and Co^{3+} species, and the nearby Co site can facilitate H adsorption, eventually completing the HER process.[21]

Besides tailoring the morphology, the fabrication of Co-based hybrid materials can boost the catalytic performance by taking advantage of the strong coupling effects between different components.[24,28] NiFe layered-double-hydroxide (NiFe-LDH) is probably one of the most ideal candidates for the construction of Co-based (*e.g.* $Co_{0.85}Se$ nanosheets) hybrids owing to its inherent catalytic activity for both the OER and HER associated with the unique layered structure.[29] In this work, for the first time, we report the synthesis of a three-dimensional (3D) strongly coupled ternary hybrid, in which $Co_{0.85}Se$ nanosheet array and NiFe-LDH are successively grown on the electrochemically exfoliated graphene (EG) foil (EG/$Co_{0.85}Se$/NiFe-LDH). In such a hybrid system, NiFe-LDH nanosheets with an average thickness of ~10 nm are uniformly anchored onto the surface of $Co_{0.85}Se$ nanosheet array that are ~30 nm thick with a few micrometers in lateral length and perpendicular to the EG foil, in which the graphene nanosheets are highly exfoliated. As a result of the 3D structure with a high surface area (156 $m^2\ g^{-1}$), a strong coupling effect among different components, and open-channels for facile electrolyte transport, the resulting EG/$Co_{0.85}Se$/NiFe-LDH hybrid not only exhibits outstanding OER performance with low overpotential (150 and 250 mA cm^{-2} at 1.50 and 1.51 V), small Tafel slope of 57 mV dec^{-1}, and excellent stability (>10 h), ranking among the most active non-precious OER catalysts, but also effectively catalyzes the HER in basic media. Importantly, an alkaline water electrolyzer in a two-electrode configuration is fabricated, which requires a cell voltage of 1.71 V to reach 20 mA cm^{-2}. This performance is well comparable to that of the most active integrated Pt/C//Ir/C catalysts (at 1.71 V overpotential) for the overall water splitting.

The fabrication process for the EG/$Co_{0.85}Se$/NiFe-LDH hybrid is illustrated in Fig. S1 (ESI†). EG was first prepared *via* an electrochemical exfoliation treatment on graphite foil in $(NH_4)_2SO_4$ according to our previous report.[30] The exfoliation time showed a considerable influence on the morphology and final catalytic activity of EG (Fig. S2, ESI†), and the optimal exfoliation time was found to be 15 s. Subsequently, the obtained EG was employed as a scaffold for the controlled growth of $Co_{0.85}Se$ nanosheet array, which was further coated by NiFe-LDH nanosheets *via* a hydrothermal treatment to form the final product of the EG/$Co_{0.85}Se$/NiFe-LDH hybrid (see the ESI† for details). The loading amount of NiFe-LDH nanosheets could be readily controlled by changing the NiFe-LDH precursor concentration. Obviously, both increasing and decreasing the concentration of the NiFe-LDH precursor caused the decrease of catalytic activity (Fig. S3, ESI†). The most optimal synthesis condition gave a material that is denoted hereafter as EG/$Co_{0.85}Se$/NiFe-LDH, unless indicated otherwise.

Fig. 1a and b show the field emission scanning electron microscopy (FESEM) images for EG, in which the edge of graphite foil was expanded and a large amount of graphene flakes were exfoliated to form a network of graphene ripples on the surface of graphite foil. Considering that the electrochemical exfoliation process is simple, the fabrication method can easily be scaled up depending on the type and size of the graphite electrode used. For example, a large-size EG foil (15 × 15 cm^2) or flexible EG can be constructed just by using a large graphite foil or a flexible graphite substrate as an electrode (Fig. S4, ESI†). For EG/$Co_{0.85}Se$, FESEM images reveal that the EG is uniformly covered by the $Co_{0.85}Se$ nanosheets with a thickness of ~30 nm and a lateral length of a few micrometers (Fig. 1c). Moreover, the $Co_{0.85}Se$ nanosheets appear to be vertically grown on the EG and spatially interconnected (Fig. S5, ESI†). A closer FESEM observation further discloses that the as-grown nanosheets are open structures and are well attached onto the EG surface (Fig. 1d). The FESEM images of the EG/$Co_{0.85}Se$/NiFe-LDH demonstrate that numerous layered NiFe-LDHs with an average thickness of ~10 nm are directly grown on the surface of EG/$Co_{0.85}Se$ nanoarray, resulting in a strong interface contact between NiFe-LDH and $Co_{0.85}Se$ on the EG (Fig. 1e, f and Fig. S5, ESI†), which can be further confirmed by Fourier transform infrared (FTIR) and X-ray photoelectron spectroscopy (XPS, see below) studies, thus guaranteeing the fast electron transfer between EG/$Co_{0.85}Se$ and NiFe-LDH. The corresponding energy-dispersive X-ray spectrum (EDX, Fig. S6, ESI†)

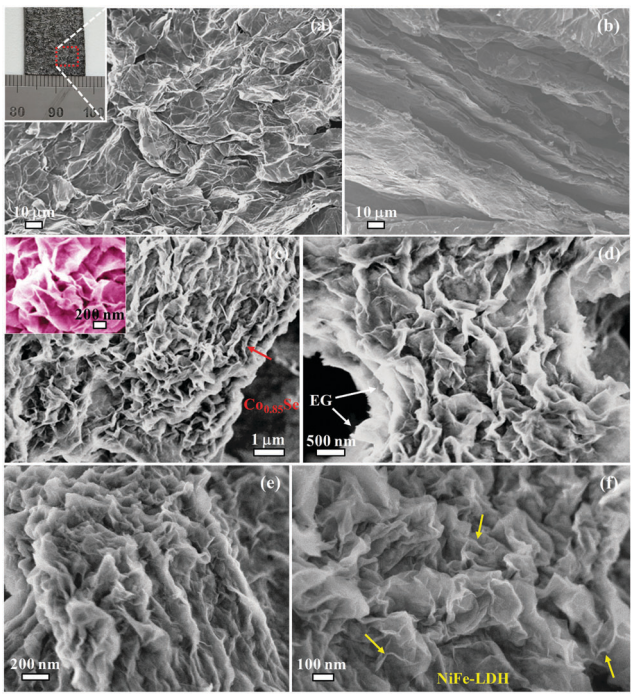

Fig. 1 FESEM images of EG (a and b), EG/$Co_{0.85}Se$ (c and d), and EG/$Co_{0.85}Se$/NiFe-LDH (e and f). Inset: The corresponding EG photograph (a) and the enlarged FESEM image of EG/$Co_{0.85}Se$ (c).

analysis validates the formation of the EG/$Co_{0.85}Se$/NiFe-LDH hybrid with Co, Se, Ni, Fe, O, and C as the principal elemental components. The elemental mapping of the EG/$Co_{0.85}Se$/NiFe-LDH further confirms the existence of the above-mentioned elements and their well-defined spatial distribution in the hybrid (Fig. S7, ESI†). Moreover, the hybrid is highly hydrophilic in nature with a small contact angle of $\sim 0.8^{\circ}$, in contrast to 13.1° and 55.6° for the EG and active carbon paper (ACP, Fig. S8, ESI†), respectively.

Further information about the microstructure of the samples was obtained from transmission electron microscopy (TEM). The TEM image of EG/$Co_{0.85}Se$ shows that the $Co_{0.85}Se$ nanosheets are anchored on the surface of large sized EG supports and the corresponding selected area electron diffraction (SAED) pattern indicates that the $Co_{0.85}Se$ nanosheets have a good crystalline structure (Fig. S9, ESI†). After the hybridization with NiFe-LDH, the black stripes corresponding to the NiFe-LDH nanosheets are observed in the hybrid by comparing the morphology of EG/$Co_{0.85}Se$/NiFe-LDH with those of EG/$Co_{0.85}Se$ and NiFe-LDH (Fig. 2a and Fig. S9, ESI†). The high-resolution TEM (HRTEM) images show the NiFe-LDH grown intimately on the $Co_{0.85}Se$ nanosheets (Fig. 2b and c), which reveal the resolved lattice fringe of the NiFe-LDH (012) plane with a spacing of 0.25 nm, as well as the (101) plane of supported hexagonal $Co_{0.85}Se$ with a spacing of 0.27. The above results are well consistent with the mixed phases probed by X-ray diffraction (XRD) which confirm the coexistence of crystalline graphitic carbon,[31] hexagonal phase $Co_{0.85}Se$ (JCPDS 52-1008), and NiFe-LDH (Fig. S10, ESI†).[32,33] Raman spectroscopy exhibits the characteristic peaks of $Co_{0.85}Se$ at 172 cm^{-1}, NiFe-LDH at 479 and 656 cm^{-1}, and the D (1325 cm^{-1}) and G (1550 cm^{-1}) bands of EG in the hybrid (Fig. S11, ESI†). The calculated peak intensity ratio (I_D/I_G) is only 0.11, indicating a low degree of defects in the EG.[34,35] The band shifts in the FTIR spectra of EG/$Co_{0.85}Se$/NiFe-LDH compared with those of EG/$Co_{0.85}Se$ and NiFe-LDH suggest the strong coupling interactions between $Co_{0.85}Se$ and NiFe-LDH (Fig. S12, ESI†).[36] Likewise, a dramatic up-shift of the characteristic FTIR bands was observed after growing $Co_{0.85}Se$ nanosheet array on the EG (Fig. S12, ESI†), probably due to the formation of interfacial covalent C–O···Co–Se bonding.[37,38] The strong chemical coupling could enable an optimized electronic structure of $Co_{0.85}Se$ upon its synergistic interaction with EG, which facilitates rapid charge transfer between $Co_{0.85}Se$ and EG as evidenced by the reduced charge transfer resistance (Fig. S12, ESI†),[11,39] compared to the physically mixed counterpart. The XPS spectra reveal that the EG/$Co_{0.85}Se$/NiFe-LDH contains the elements of C, O, Co, Se, Ni, and Fe, and the atomic ratio of Ni/Fe is about 3 : 1 (Fig. S13 and S14, ESI†), confirming the composition of NiFe-LDH along with the XRD result. The atomic ratio of Co/Se in the EG/$Co_{0.85}Se$/NiFe-LDH was calculated to be $\sim$0.85 from inductively coupled plasma–optic emission spectrometry (ICP-OES) measurements, which supports the formation of hexagonal $Co_{0.85}Se$. In comparison to the XPS peak centered at 780.3 eV assigned to Co $2p_{3/2}$ in EG/$Co_{0.85}Se$ (Fig. 2d), an obvious down-shift of the corresponding peak in EG/$Co_{0.85}Se$/NiFe-LDH to 779.6 eV is identified, suggesting a strong electron transfer from NiFe-LDH to $Co_{0.85}Se$.[40,41]

The N_2 adsorption isotherm of the EG/$Co_{0.85}Se$/NiFe-LDH shows a typical type IV curve with an H3-type of hysteresis loop, representing the slit mesopores generated from sheet-like aggregation (Fig. 2e).[42] The Brunauer–Emmett–Teller (BET) surface area of the hybrid was measured to be 156 $m^2\ g^{-1}$ with a relatively wide pore size distribution in the range of 2–20 nm. The surface area is much larger than that of the EG (15 $m^2\ g^{-1}$), EG/$Co_{0.85}Se$ (65 $m^2\ g^{-1}$), and EG/NiFe-LDH (73 $m^2\ g^{-1}$), as well as other reported vertically-oriented inorganic nanosheets (or nanowires) (up to $\sim$120 $m^2\ g^{-1}$, Table S1, ESI†). The high surface area would provide rich active sites and large contact areas for the electrocatalytic process.

Next, the EG/$Co_{0.85}Se$/NiFe-LDH was directly used as an electrode to catalyze the OER (Fig. S15, ESI†) in a typical three-electrode setup in 1.0 M aqueous KOH solution. For comparison, EG, EG/$Co_{0.85}Se$, EG/NiFe-LDH, and Ir/C were also investigated under the same conditions. Potentials are reported *versus* the reversible hydrogen electrode (RHE). Prior to water oxidation (before the onset of OER), the oxidation peak at around 1.43 V observed for EG/$Co_{0.85}Se$/NiFe-LDH can be assigned to the transformation of Ni(II) to Ni (III or IV) species,[43] which is believed to be the active site of NiFe-LDH-based materials for the OER.[19,33] The EG/$Co_{0.85}Se$/NiFe-LDH exhibited a remarkably high activity with an onset potential of 1.47 V (the start of water oxidation,[44] Fig. 3a), which was more negative than its counterparts (1.65 V for EG, 1.58 V for EG/$Co_{0.85}Se$, and 1.49 V for EG/NiFe-LDH). This onset potential was even about 100 mV lower than that of the commercial Ir/C catalyst. The excellent activity of EG/$Co_{0.85}Se$/NiFe-LDH was further confirmed by its explicitly higher current density than that of other reference samples over the entire potential range measured. For example, the current density of the ternary hybrid at 1.52 V reached 270.9 mA cm^{-2}, which was much higher than those of EG/$Co_{0.85}Se$ (11.5 mA cm^{-2}), EG/NiFe-LDH (48.2 mA cm^{-2}), and Ir/C ($\sim$0 mA cm^{-2}), respectively, and even much better than that of the most previous reports under similar conditions (current density up to $\sim$200 mA cm^{-2} at 1.5 V).[19–20,45,46] Moreover, the mass activities of EG/$Co_{0.85}Se$/NiFe-LDH, EG/$Co_{0.85}Se$, and EG/NiFe-LDH at 1.52 V

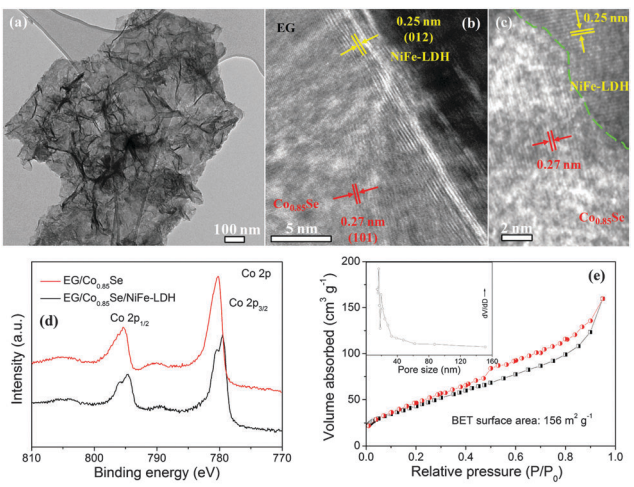

Fig. 2 TEM (a) and HRTEM (b and c) images of EG/$Co_{0.85}Se$/NiFe-LDH. (d) High-resolution Co 2p XPS spectra of EG/$Co_{0.85}Se$ and EG/$Co_{0.85}Se$/NiFe-LDH. (e) N_2 adsorption isotherm and the corresponding pore size distribution (inset) of EG/$Co_{0.85}Se$/NiFe-LDH.

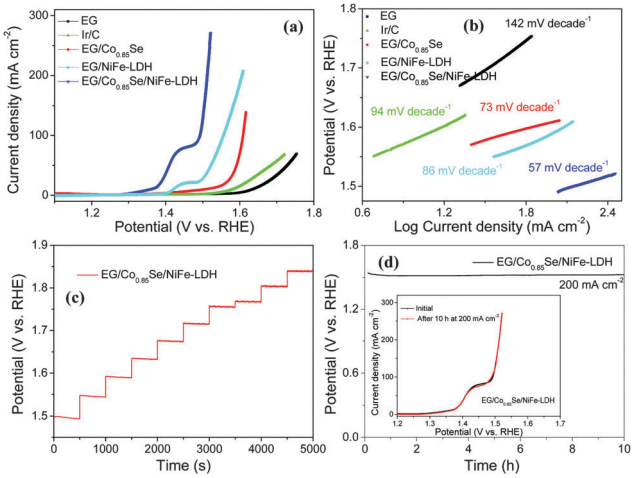

Fig. 3 (a) Polarization curves for EG, EG/$Co_{0.85}Se$, EG/NiFe-LDH, EG/$Co_{0.85}Se$/NiFe-LDH, and Ir/C for the OER. (b) The corresponding Tafel plots. (c) Multi-current process of EG/$Co_{0.85}Se$/NiFe-LDH. The current density started at 50 mA cm^{-2} and finished at 500 mA cm^{-2}, with an increment of 50 mA cm^{-2} every 500 s without iR correction. (d) Chronopotentiometry curve of the EG/$Co_{0.85}Se$/NiFe-LDH under high current density of 200 mA cm^{-2} without iR correction; inset: polarization curves of EG/$Co_{0.85}Se$/NiFe-LDH before and after chronopotentiometry measurement at a current density of 200 mA cm^{-2} for about 10 h. All experiments were carried out in 1.0 M KOH.

were calculated to be 67.7, 4.3, and 14.6 mA mg^{-1}, respectively. Of note, bare EG foil with a small amount of oxygen functional groups and few structural defects[47] (Fig. S16 and S17, ESI†) contribute to the partial catalytic activity (Fig. 3a and Fig. S2, ESI†) in the hybrid, which is different from traditional substrates (such as Ni foam,[48] ACP (Fig. S18, ESI†), and glassy carbon electrodes[49]) with negligible activity. The C atoms adjacent to the substituted oxygen groups may function as active sites by redistributing their charge and spin density for water dissociation[50] due to the high electro-negativity of O species (Fig. S2, ESI†).[51] Besides, the above OER results demonstrate that both EG/$Co_{0.85}Se$ and EG/NiFe-LDH have higher catalytic activity than the EG (Fig. 3a), indicating that both $Co_{0.85}Se$ and NiFe-LDH can be the active centers to boost the OER. Since the activity of EG/$Co_{0.85}Se$ without NiFe-LDH only accounts 6.4% of the hybrid according to the mass activity at 1.52 V, the NiFe-LDH should be the main active species in the EG/$Co_{0.85}Se$/NiFe-LDH for catalyzing the OER.

For driving a current density of 150 mA cm^{-2}, the commercial Ir/C catalyst requires an overpotential of more than 1.80 V. As a comparison, the OER activity of EG/$Co_{0.85}Se$/NiFe-LDH outperforms this noble metal, with merely 1.50 and 1.51 V to achieve the current densities of 150 and 250 mA cm^{-2}, respectively. Such performance is not only greater than that of most of the previously reported non-precious metal OER electrocatalysts (Table S2, ESI†), but also superior to those reported for other nanoarray electrodes such as $Ni_xCo_{3-x}O_4$ nanowire array/Ti foil (1.60 V at 10 mA cm^{-2}, 1.0 M NaOH),[52] NiFe-LDH nanoplatelet array/Ni foam (1.69 V at 150 mA cm^{-2}, 1.0 M KOH),[48] $Zn_xCo_{3-x}O_4$ nanowire array/Ti foil (1.55 V at 10 mA cm^{-2}, 1.0 M KOH),[46] and NiSe nanowire/Ni foam (1.57 V at 150 mA cm^{-2}, 1.0 M KOH).[53]

Further catalytic kinetics evaluation can be seen from the Tafel plots (Fig. 3b). The EG/$Co_{0.85}Se$/NiFe-LDH exhibited favorable kinetics toward the OER with a low Tafel slope of 57 mV dec^{-1} in contrast to those of EG (142 mV dec^{-1}), EG/$Co_{0.85}Se$ (73 mV dec^{-1}), EG/NiFe-LDH (86 mV dec^{-1}), and Ir/C (94 mV dec^{-1}), respectively. Fig. 3c shows a multi-step chronopotentiometric curve for EG/$Co_{0.85}Se$/NiFe-LDH. The potential immediately levels off at 1.50 V at the start of 50 mA cm^{-2}, and remains constant for the rest 500 s; the other steps also show similar results up to 500 mA cm^{-2}, implying the excellent mass transport properties and mechanical robustness of EG/$Co_{0.85}Se$/NiFe-LDH.[45] The resistance measured by a four-point probe system revealed the values of 0.24, 2.7, 5.1, and 3.3 kΩ sq^{-1} for EG, EG/$Co_{0.85}Se$, EG/NiFe-LDH, and EG/$Co_{0.85}Se$/NiFe-LDH, respectively (Fig. S19, ESI†). The EG/$Co_{0.85}Se$/NiFe-LDH has a lower conductivity (higher resistance) but a higher catalytic activity than EG and EG/$Co_{0.85}Se$, confirming that the introduced NiFe-LDH contributed to the improvement of the overall catalytic activity. Fig. 3d presents the impressive OER stability of EG/$Co_{0.85}Se$/NiFe-LDH, with 200 mA cm^{-2} anodic current at ~1.52 V for over 10 h without obvious degradation. Moreover, the ternary hybrid maintained nearly the similar polarization curve after the chronopotentiometry measurement for 10 h (inset of Fig. 3d).

Afterwards, we examined the electrocatalytic activity of EG/$Co_{0.85}Se$/NiFe-LDH for the HER in 1.0 M KOH (Fig. S20, ESI†). EG/$Co_{0.85}Se$/NiFe-LDH exhibited a high electrocatalytic activity with a small onset potential of −0.24 V (Fig. 4a), beyond which the cathodic current density rose rapidly under more negative potentials with substantial current density of 13.6 mA cm^{-2} at −0.3 V. In contrast, either EG/$Co_{0.85}Se$ or EG/NiFe-LDH exhibited inferior HER activity with a higher onset overpotential (−0.26 or −0.35 V) and lower cathodic current density (8.37 or 3.06 mA cm^{-2} at −0.3 V). It is noteworthy that the EG/NiFe-LDH accounts only for about 22.5% activity of EG/$Co_{0.85}Se$/NiFe-LDH (13.6 *vs.* 3.06 mA cm^{-2} at −0.3 V) and the onset overpotential of EG/NiFe-LDH is more negative than that of EG/$Co_{0.85}Se$. This suggests that EG/$Co_{0.85}Se$ should be the main contributor of active sites for catalyzing the HER. That is, EG/$Co_{0.85}Se$ not only serves as the 3D scaffold on which the hybrid electrode can be fabricated, but also plays a role as HER active material. Moreover, the EG/$Co_{0.85}Se$/NiFe-LDH showed overpotentials of −0.21 and −0.26 V at current densities of 5 and 10 mA cm^{-2}, respectively, which is favorably comparable with that of many previously reported noble metal-free HER electrocatalysts in basic media, including recently developed Co (Fe, or Ni)-based catalysts as well as some MoS_2-based catalysts (Fig. S21, ESI†). The Tafel slope and exchange current density (calculated by extrapolation using the Tafel plot,[54] and reflected intrinsic rates of electron transfer between the solution and electrode[55]) of EG/$Co_{0.85}Se$/NiFe-LDH were determined to be 160 mV dec^{-1} and 0.22 mA cm^{-2}, respectively. The values are compared with other samples such as EG/$Co_{0.85}Se$ (223 mV dec^{-1}, 0.40 mA cm^{-2}) and EG/NiFe-LDH (125 mV dec^{-1}, 0.025 mA cm^{-2}), implying a more rapid HER rate for the EG/$Co_{0.85}Se$/NiFe-LDH electrode (Fig. S22, ESI†).[56,57] Moreover, the ternary hybrid showed a similar polarization curve after 1000 cycles compared with the initial one (Fig. 4b), with negligible loss of cathodic current density, confirming the excellent stability of the EG/$Co_{0.85}Se$/NiFe-LDH towards the HER

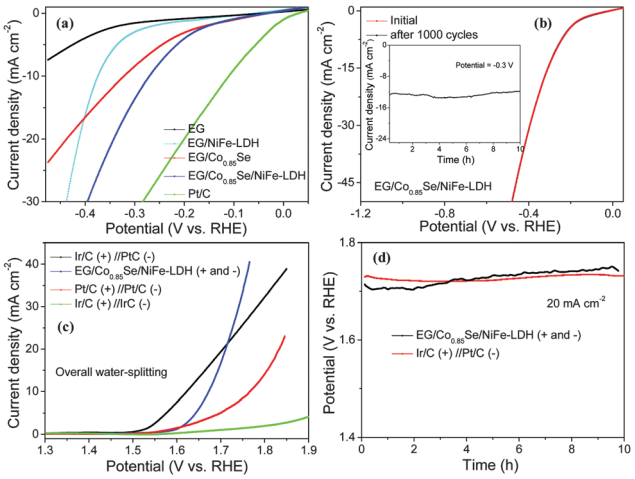

Fig. 4 (a) Polarization curves for EG, EG/$Co_{0.85}Se$, EG/NiFe-LDH, EG/$Co_{0.85}Se$/NiFe-LDH, and Pt/C for the HER. (b) Polarization curves of EG/$Co_{0.85}Se$/NiFe-LDH before and after 1000 CV cycles. Inset: Chronoamperometry curve of the EG/$Co_{0.85}Se$/NiFe-LDH at a constant potential of −0.3 V without iR correction. (c) Polarization curves of EG/$Co_{0.85}Se$/NiFe-LDH, Ir/C (+)//Ir/C (−), Pt/C (+)//Pt/C (−), and Ir/C (+)//Pt/C (−) for overall water splitting in a two-electrode configuration. (d) Chronopotentiometry curves of the EG/$Co_{0.85}Se$/NiFe-LDH and Ir/C (+)//Pt/C (−) under a current density of 20 mA cm^{-2} without iR correction. All experiments were carried out in 1.0 M KOH.

in alkaline media. The time-dependent current density curve at a fixed potential of −0.3 V manifested that the hybrid maintained its catalytic activity for at least 10 h of continuous operation (the inset of Fig. 4b).

Encouraged by the excellent OER and HER results, we accordingly assembled a water electrolyzer in 1.0 M KOH, whose anode and cathode both comprised EG/$Co_{0.85}Se$/NiFe-LDH. Continuous gas bubbling was observed on both electrodes throughout the test (Fig. S23, ESI†). Remarkably enough, the overall water-splitting using EG/$Co_{0.85}Se$/NiFe-LDH required a lower overpotential of 1.67 V to afford 10 mA cm^{-2} (1.71 V at 20 mA cm^{-2}, Fig. 4c), in contrast to over 1.90 V overpotential for Ir/C//Ir/C electrodes and over 1.75 V overpotential for Pt/C//Pt/C electrodes (Table S3, ESI†). Although the overpotential values (1.67 and 1.71 V at 10 and 20 mA cm^{-2}) of the EG/$Co_{0.85}Se$/NiFe-LDH hybrid are slightly larger than those of the benchmark combination catalyst (Ir/C (anode)//Pt/C (cathode), 1.62 and 1.71 V at 10 and 20 mA cm^{-2}), the ternary hybrid exhibited superior stability in the long-term electrochemical process. For instance, at a current density of 20 mA cm^{-2}, the overpotential of EG/$Co_{0.85}Se$/NiFe-LDH remained stable at ∼1.73 V for electrolysis over 10 h (Fig. 4d). In contrast, the overpotential of Ir/C (+, anode)//Pt/C (−, cathode) increased considerably from 1.71 V to 1.75 V (∼40 mV shift at 20 mA cm^{-2}) during 10 h.

The high activity and excellent stability of the 3D EG/$Co_{0.85}Se$/NiFe-LDH can be attributed to the following aspects: (I) intrinsic merits and strong coupling effects of the three components contribute to the high activity and stability. The *in situ* growth of $Co_{0.85}Se$ nanosheet array and NiFe-LDH on the EG foil enables intimate contact and strong adhesion in the hybrid. No obvious change on the structure and chemical composition of the hybrid before and after electrochemical water splitting tests was observed based on XRD and XPS studies (Fig. S24 and S13, ESI†). (II) The direct integration of NiFe-LDH on $Co_{0.85}Se$ nanosheets grown on EG ensures efficient charge transport among three components in the hybrid, which can be confirmed by electrochemical impedance spectroscopy (EIS) studies (Fig. S25 and S26, ESI†). The ternary hybrid exhibits a much lower charge transfer resistance than the physical mixture of EG, $Co_{0.85}Se$, and NiFe-LDH, suggesting that more effective shuttling of charges occurs at the heterostructure interfaces. (III) The unique nanoarray structure favors fast vectorial electron-transport along the nanosheets to current collectors,[56] which is supported by the results that the EG/$Co_{0.85}Se$/NiFe-LDH foil exhibits much higher OER activity than its powder-like counterpart (obtained by scratching down the hybrid from graphite foil, Fig. S27, ESI†). (IV) The 3D hierarchical structure of the vertically oriented EG/$Co_{0.85}Se$/NiFe-LDH nanosheets with high surface area ensures abundant open spaces, which facilitate the diffusion of electrolyte into the active sites and promote rapid release of as-formed gas bubbles.

Conclusions

In summary, a 3D strongly coupled ternary hybrid of EG/$Co_{0.85}Se$/NiFe-LDH was fabricated by anchoring NiFe-LDH onto the $Co_{0.85}Se$ nanosheets vertically aligned on the EG foil. This hierarchical hybrid exhibited excellent OER activity with overpotentials of 1.50 and 1.51 V at current densities of 150 and 250 mA cm^{-2}, respectively, which were more active than those reported for other non-precious metal OER materials and state-of-art Ir/C catalysts in an alkaline electrolyte. Together with the high HER performance for EG/$Co_{0.85}Se$/NiFe-LDH nanosheets, it is remarkable that an efficient water electrolyzer was demonstrated by using the ternary hybrid as both an anode and a cathode, achieving 20 mA cm^{-2} at 1.71 V, which was well comparable to that of the benchmark combination catalyst (Ir/C (+, anode)//Pt/C (−, cathode), 1.71 V at 20 mA cm^{-2}). The developed 3D EG-supported hybrid consisting of transition metal dichalcogenides and complex metal oxide may provide an important platform for further developing a variety of functional applications, such as in photoelectrocatalysis, supercapacitor, and fuel cells.

Acknowledgements

This work was financially supported by the ERC Grant 2DMATER, the CFAED, and the EC under the Graphene Flagship (no. CNECT-ICT-604391). We acknowledge support from Dr Petr Formanek for TEM measurements.

Notes and references

1 Y. Jiao, Y. Zheng, M. Jaroniec and S. Z. Qiao, *Chem. Soc. Rev.*, 2015, **44**, 2060–2086.
2 J. Luo, J. H. Im, M. T. Mayer, M. Schreier, M. K. Nazeeruddin, N. G. Park, S. D. Tilley, H. J. Fan and M. Grätzel, *Science*, 2014, **345**, 1593–1596.

3 J. Suntivich, K. J. May, H. A. Gasteiger, J. B. Goodenough and Y. Shao-Horn, *Science*, 2011, **334**, 1383–1385.
4 D. Voiry, H. Yamaguchi, J. Li, R. Silva, D. C. B. Alves, T. Fujita, M. Chen, T. Asefa, V. B. Shenoy, G. Eda and M. Chhowalla, *Nat. Mater.*, 2013, **12**, 850–855.
5 M. G. Walter, E. L. Warren, J. R. McKone, S. W. Boettcher, Q. Mi, E. A. Santori and N. S. Lewis, *Chem. Rev.*, 2010, **110**, 6446–6473.
6 J. I. Jung, H. Y. Jeong, J. S. Lee, M. G. Kim and J. Cho, *Angew. Chem., Int. Ed.*, 2014, **53**, 4582–4586.
7 S. Gupta, W. Kellogg, H. Xu, X. Liu, J. Cho and G. Wu, *Chem. – Asian J.*, 2015, DOI: 10.1002/asia.201500640.
8 T. Maiyalagan, K. A. Jarvis, S. Therese, P. J. Ferreira and A. Manthiram, *Nat. Commun.*, 2014, **5**, 3949.
9 J. Kibsgaard, Z. Chen, B. N. Reinecke and T. F. Jaramillo, *Nat. Mater.*, 2012, **11**, 963–969.
10 J. Tian, Q. Liu, N. Cheng, A. M. Asiri and X. Sun, *Angew. Chem., Int. Ed.*, 2014, **53**, 9577–9581.
11 Y. R. Zheng, M. R. Gao, Z. Y. Yu, Q. Gao, H. L. Gao and S. H. Yu, *Chem. Sci.*, 2015, **6**, 4594–4598.
12 H. Vrubel and X. Hu, *Angew. Chem.*, 2012, **124**, 12875–12878.
13 W. F. Chen, J. T. Muckerman and E. Fujita, *Chem. Commun.*, 2013, **49**, 8896–8909.
14 C. Tan and H. Zhang, *Chem. Soc. Rev.*, 2015, **44**, 2713–2731.
15 Y. Yan, B. Y. Xia, X. Ge, Z. Liu, A. Fisher and X. Wang, *Chem. – Eur. J.*, 2015, **21**, 18062–18067.
16 Y. Yan, L. Thia, B. Y. Xia, X. Ge, Z. Liu, A. Fisher and X. Wang, *Adv. Sci.*, 2015, **2**, 1500120.
17 X. Zou, X. Huang, A. Goswami, R. Silva, B. R. Sathe, E. Mikmeková and T. Asefa, *Angew. Chem.*, 2014, **126**, 4461–4465.
18 D. Merki, S. Fierro, H. Vrubel and X. Hu, *Chem. Sci.*, 2011, **2**, 1262.
19 H. Wang, H. W. Lee, Y. Deng, Z. Lu, P. C. Hsu, Y. Liu, D. Lin and Y. Cui, *Nat. Commun.*, 2015, **6**, 7261.
20 Y. Yang, H. Fei, G. Ruan and J. M. Tour, *Adv. Mater.*, 2015, **27**, 3175–3180.
21 H. Jin, J. Wang, D. Su, Z. Wei, Z. Pang and Y. Wang, *J. Am. Chem. Soc.*, 2015, **137**, 2688–2694.
22 M. R. Gao, Y. F. Xu, J. Jiang and S. H. Yu, *Chem. Soc. Rev.*, 2013, **42**, 2986–3017.
23 F. Gong, H. Wang, X. Xu, G. Zhou and Z. S. Wang, *J. Am. Chem. Soc.*, 2012, **134**, 10953–10958.
24 M. R. Gao, J. X. Liang, Y. R. Zheng, Y. F. Xu, J. Jiang, Q. Gao, J. Li and S. H. Yu, *Nat. Commun.*, 2015, **6**, 5982.
25 M. R. Gao, X. Cao, Q. Gao, Y. F. Xu, Y. R. Zheng, J. Jiang and S. H. Yu, *ACS Nano*, 2014, **8**, 3970–3978.
26 L. F. Zhang and C. Y. Zhang, *Nanoscale*, 2014, **6**, 1782–1789.
27 S. Cao, Y. Chen, L. Kang, Z. Lin and W. F. Fu, *J. Mater. Chem. A*, 2015, **3**, 18711–18717.
28 J. Zhang, M. Grzelczak, Y. Hou, K. Maeda, K. Domen, X. Fu, M. Antonietti and X. Wang, *Chem. Sci.*, 2012, **3**, 443–446.
29 M. Gong and H. Dai, *Nano Res.*, 2015, **8**, 23–39.
30 K. Parvez, Z. S. Wu, R. Li, X. Liu, R. Graf, X. Feng and K. Müllen, *J. Am. Chem. Soc.*, 2014, **136**, 6083–6091.
31 J. G. Ren, Q. H. Wu, H. Tang, G. Hong, W. Zhang and S. T. Lee, *J. Mater. Chem. A*, 2013, **1**, 1821–1826.
32 J. F. Zhao, J. M. Song, C. C. Liu, B. H. Liu, H. L. Niu, C. J. Mao, S. Y. Zhang, Y. H. Shen and Z. P. Zhang, *CrystEngComm*, 2011, **13**, 5681–5684.
33 M. Gong, Y. Li, H. Wang, Y. Liang, J. Z. Wu, J. Zhou, J. Wang, T. Regier, F. Wei and H. Dai, *J. Am. Chem. Soc.*, 2013, **135**, 8452–8455.
34 K. R. Paton, E. Varrla, C. Backes, R. J. Smith, U. Khan, A. O'Neill, C. Boland, M. Lotya, O. M. Istrate, P. King, T. Higgins, S. Barwich, P. May, P. Puczkarski, I. Ahmed, M. Moebius, H. Pettersson, E. Long, J. Coelho, S. E. O'Brien, E. K. McGuire, B. M. Sanchez, G. S. Duesberg, N. McEvoy, T. J. Pennycook, C. Downing, A. Crossley, V. Nicolosi and J. N. Coleman, *Nat. Mater.*, 2014, **13**, 624–630.
35 A. Ciesielski and P. Samori, *Chem. Soc. Rev.*, 2014, **43**, 381–398.
36 T. Y. Ma, J. Ran, S. Dai, M. Jaroniec and S. Z. Qiao, *Angew. Chem., Int. Ed.*, 2015, **54**, 4646–4650.
37 C. Tang, H. S. Wang, H. F. Wang, Q. Zhang, G. L. Tian, J. Q. Nie and F. Wei, *Adv. Mater.*, 2015, **27**, 4516–4522.
38 Y. Liang, Y. Li, H. Wang, J. Zhou, J. Wang, T. Regier and H. Dai, *Nat. Mater.*, 2011, **10**, 780–786.
39 D. Tang, J. Liu, X. Wu, R. Liu, X. Han, Y. Han, H. Huang, Y. Liu and Z. Kang, *ACS Appl. Mater. Interfaces*, 2014, **6**, 7918–7925.
40 Y. R. Zheng, M. R. Gao, Q. Gao, H. H. Li, J. Xu, Z. Y. Wu and S. H. Yu, *Small*, 2015, **11**, 182–188.
41 M. R. Gao, Y. F. Xu, J. Jiang, Y. R. Zheng and S. H. Yu, *J. Am. Chem. Soc.*, 2012, **134**, 2930–2933.
42 D. Gu and F. Schuth, *Chem. Soc. Rev.*, 2014, **43**, 313–344.
43 M. W. Louie and A. T. Bell, *J. Am. Chem. Soc.*, 2013, **135**, 12329–12337.
44 X. Long, J. Li, S. Xiao, K. Yan, Z. Wang, H. Chen and S. Yang, *Angew. Chem., Int. Ed.*, 2014, **53**, 7584–7588.
45 X. Lu and C. Zhao, *Nat. Commun.*, 2015, **6**, 4345.
46 X. Liu, Z. Chang, L. Luo, T. Xu, X. Lei, J. Liu and X. Sun, *Chem. Mater.*, 2014, **26**, 1889–1895.
47 Z. Y. Xia, S. Pezzini, E. Treossi, G. Giambastiani, F. Corticelli, V. Morandi, A. Zanelli, V. Bellani and V. Palermo, *Adv. Funct. Mater.*, 2013, **23**, 4684–4693.
48 Z. Li, M. Shao, H. An, Z. Wang, S. Xu, M. Wei, D. G. Evans and X. Duan, *Chem. Sci.*, 2015, **6**, 6624–6631.
49 F. Song and X. Hu, *J. Am. Chem. Soc.*, 2014, **136**, 16481–16484.
50 J. Duan, S. Chen, B. A. Chambers, G. G. Andersson and S. Z. Qiao, *Adv. Mater.*, 2015, **27**, 4234–4241.
51 S. Chen, J. Duan, J. Ran, M. Jaroniec and S. Z. Qiao, *Energy Environ. Sci.*, 2013, **6**, 3693–3699.
52 Y. Li, P. Hasin and Y. Wu, *Adv. Mater.*, 2010, **22**, 1926–1929.
53 C. Tang, N. Cheng, Z. Pu, W. Xing and X. Sun, *Angew. Chem., Int. Ed.*, 2015, **54**, 9351–9355.
54 H. W. Liang, S. Bruller, R. Dong, J. Zhang, X. Feng and K. Mullen, *Nat. Commun.*, 2015, **6**, 7992.
55 D. Tang, J. Lu, L. Zhuang and P. Liu, *J. Electroanal. Chem.*, 2010, **644**, 144–149.
56 Y. Hou, F. Zuo, A. Dagg and P. Feng, *Angew. Chem., Int. Ed.*, 2013, **52**, 1248–1252.
57 J. Xie, S. Li, X. Zhang, J. Zhang, R. Wang, H. Zhang, B. Pan and Y. Xie, *Chem. Sci.*, 2014, **5**, 4615–4620.